



Contents lists available at ScienceDirect

# Bioorganic & Medicinal Chemistry Letters

journal homepage: [www.elsevier.com/locate/bmcl](http://www.elsevier.com/locate/bmcl)

## Discovery and optimization of indazoles as potent and selective interleukin-2 inducible T cell kinase (ITK) inhibitors



Richard M. Pastor\*, Jason D. Burch, Steven Magnuson, Daniel F. Ortwine, Yuan Chen, Kelly De La Torre, Xiao Ding, Charles Eigenbrot, Adam Johnson, Marya Liimatta, Yichin Liu, Steven Shia, Xiaolu Wang, Lawren C. Wu, Zhonghua Pei

Genentech Inc., 1 DNA Way, South San Francisco, CA 94080, United States

### ARTICLE INFO

#### Article history:

Received 20 February 2014

Revised 6 April 2014

Accepted 7 April 2014

Available online 16 April 2014

#### Keywords:

SBDD

ITK

Indazole

X-ray crystallography

$\pi$ -stacking

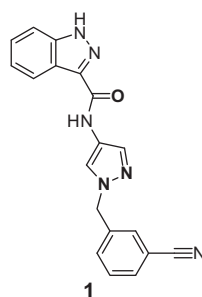
### ABSTRACT

There is evidence that small molecule inhibitors of the non-receptor tyrosine kinase ITK, a component of the T-cell receptor signaling cascade, could represent a novel asthma therapeutic class. Moreover, given the expected chronic dosing regimen of any asthma treatment, highly selective as well as potent inhibitors would be strongly preferred in any potential therapeutic. Here we report hit-to-lead optimization of a series of indazoles that demonstrate sub-nanomolar inhibitory potency against ITK with strong cellular activity and good kinase selectivity. We also elucidate the binding mode of these inhibitors by solving the X-ray crystal structures of the complexes.

© 2014 Elsevier Ltd. All rights reserved.

Interleukin-2 inducible T-cell kinase (ITK), a member of the Tec kinase family of non-receptor tyrosine kinases, plays a major role in T-cell signaling.<sup>1</sup> Along with other T-cell specific tyrosine kinases (including LCK and ZAP-70), ITK serves to amplify the signal associated with the T-cell receptor (TCR) cascade. Aberrant signaling behavior in this cascade is known to lead to autoimmune disorders and inflammation.<sup>2</sup> In studies with ITK knockout mice, levels of Th2 cytokines such as IL-4, IL-5, and IL-13 have been reduced.<sup>3</sup> Moreover, immunological symptoms of allergic asthma were attenuated in these mice and lung inflammation, eosinophil infiltration and mucous production were drastically reduced in response to challenge with the allergen ovalbumin.<sup>4</sup> These and other reports suggest that selective inhibition of ITK could represent a novel therapy for the treatment of asthma.<sup>5</sup>

In order to identify novel ITK inhibitors, a high throughput screen of our internal small molecule screening collection was conducted.<sup>6</sup> From this screen, **1** (Fig. 1) was identified as a suitable starting point for chemistry optimization. This compound was synthesized starting from methyl-1H-indazole-3-carboxylate (**2**) as described in Scheme 1. SEM protection of indazole **2** and subsequent hydrolysis of the methyl ester gave SEM protected indazole acid **3**. In parallel, 3-nitropyrazole (**4**) was reacted with 3-cyanobenzyl alcohol under standard Mitsunobu conditions<sup>7</sup> and thereaf-



ITK  $K_i$  = 43 nM  
 LE = 0.397  
 LogD<sub>7.4</sub> = 3.0 (ref. 9)  
 >50% inhibition against  
 18/75 kinases in kinase panel (ref.10)  
 > 85% inhibition against  
 6/75 kinases including JAK2  
 and FLT3<sup>10</sup>

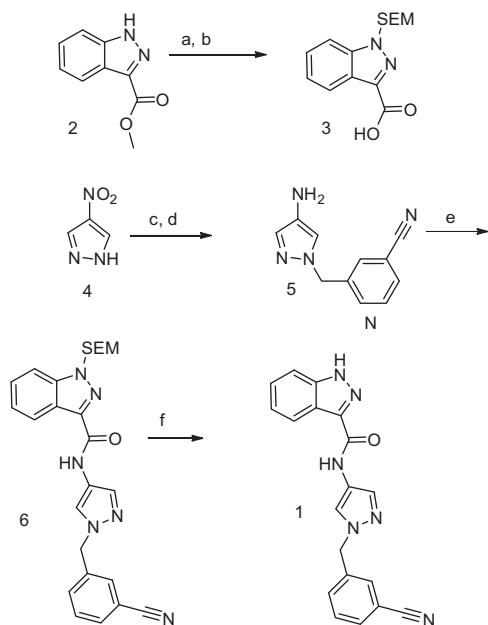
**Figure 1.** Initial indazole high-throughput screening hit. (See above-mentioned references for further information).

ter reduced to obtain 3-amino pyrazole **5**. Carboxylic acid **3** and amino-pyrazole **5** were then coupled to give amide **6**, which upon SEM deprotection afforded indazole **1**.

With **1** in hand, attempts to co-crystallize **1** with the kinase domain of ITK were taken and proved to be successful (Fig. 2). Examination of the structure revealed the central ligand-receptor interaction to consist of 3 hydrogen bonds between the hinge of the kinase domain and the indazole-carboxamide component of **1**. This then positioned the pyrazole and cyanobenzyl moieties to form  $\pi$ - $\pi$  stacking interactions with Phe-437 in face to face and edge to face manners, respectively.<sup>8</sup> In addition to the interactions

\* Corresponding author. Tel.: +1 650 225 8114.

E-mail address: [pastor.richard@gene.com](mailto:pastor.richard@gene.com) (R. M. Pastor).



Reagents and Conditions: a) SEM-Cl, NaH, THF; b) 2M LiOH, THF; c) 3-Cyanobenzyl alcohol, PPh<sub>3</sub>, DIAD, DCM; d) Fe, NH<sub>4</sub>Cl, H<sub>2</sub>O, EtOH, 70 °C for 1 hr; e) 2, HATU, DIPEA, DMF; f) TFA, DCM.

**Scheme 1.** Synthesis of inhibitor **1**.

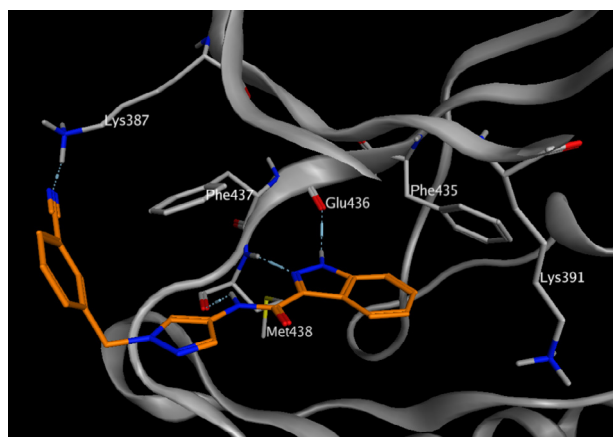
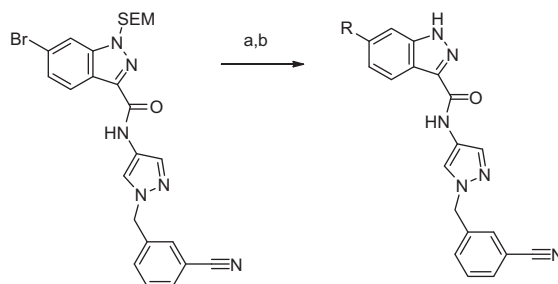


**Figure 2.** X-ray crystal structure of **1** with the kinase domain of ITK (resolution 2.6 Å, PDB code 4PP9). Protein–ligand hydrogen bonds are denoted by dashed lines with cylinders. Figure was generated using MOE ([www.chemcomp.com](http://www.chemcomp.com)).

elucidated by the crystal structure, we were also encouraged by the proximal location of the indazole-C6 to the gatekeeper Phe-435 side chain. This orientation presented an opportunity for making additional interactions with the protein in the form of  $\pi$ - $\pi$  stacking interactions with this residue.

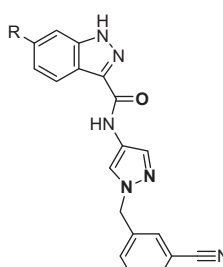
Based on the crystal structure, exploration of substitution at the indazole C6 position was undertaken. Desired analogs were synthesized via parallel Suzuki couplings according to [Scheme 2](#).<sup>11</sup> Five and six-membered aromatic and heteroaromatic rings were explored to examine the potential of forming face-to-face  $\pi$  stacking interactions with the gatekeeper ([Table 1](#)). Appending a phenyl group (**7**) resulted in a 10-fold loss in activity relative to **1**. However, substitution with a 4-pyridyl moiety (**8**) led to an equipotent analog, while a 3-pyridyl ring addition (**9**) resulted in a 4-fold potency increase. Addition of an amine to give 4-amino-3-pyridine



Reagents and Conditions: a) RB(OH)<sub>2</sub>, PdCl<sub>2</sub>(Dppf), 1M Na<sub>2</sub>CO<sub>3</sub>, ACN, 120 °C; b) TFA, DCM

**Scheme 2.** Parallel synthesis of indazole C6 substituted analogs.

**Table 1**  
SAR of Indazole C6 substituents



Example	R	K <sub>i</sub> (nM)
7		580
8		59
9		10
10		1.4
11		0.8
12		7.8

**10** resulted in a 6-fold increase in potency relative to **9**. A pyrazole was also appended to indazole C6 in both regioisomeric configurations. 4-Pyrazolyl substitution (**11**) resulted in a K<sub>i</sub> of 0.8 nM, while the 3-pyrazolyl substituted analog (**12**) demonstrated a K<sub>i</sub> of 7.8 nM. Upon obtaining a co-crystal structure of **11**, two key interactions involving the pyrazole were revealed ([Fig. 3](#)). In addition to the expected face-to-face  $\pi$ -stacking interaction with Phe-435, an H-bond with the sidechain of Lys-391 was also evident. In order to optimize the  $\pi$ -stacking interaction, the pyrazole rotates 28° out of plane with the indazole ring and calculations show this to be a low energy torsion.<sup>12</sup> Calculations also show regioisomer **12** would prefer a co-planar arrangement of the pyrazole and indazole rings. Adopting a 28 degree out of plane orientation to maximize a  $\pi$ -stacking interaction with Phe-435 would place **12** in a higher energy conformation, consistent with an 8-fold loss in potency.<sup>13</sup>

Focus then turned to optimization of the cyanobenzyl-substituted pyrazole moiety. Based on the existing crystal structures, the pyrazole and cyanobenzyl components  $\pi$  stack with Phe-437

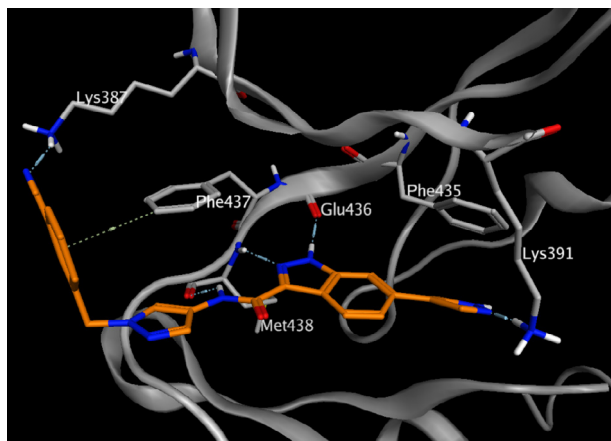


**Figure 3.** Co-crystal structure of **11** with the kinase domain of ITK (Resolution 2.7 Å, PDB code 4PPA). Protein–ligand hydrogen bonds and  $\pi$ – $\pi$  stacking interactions are denoted by dashed lines with cylinders.

in face to face and edge to face manners, respectively. The methylene group acts as the linker connecting these components, enabling the requisite interaction geometries. In order to assess the spatial and electronic details of these interactions, a variety of heterocyclic replacements of the pyrazole were tested, with significant decreases in potency observed in all cases (Table 2). The 2,5-disubstituted pyrazole **13** and 3,5-disubstituted thiazole **14** demonstrated roughly 100 fold losses in potency relative to **1**. Even larger reductions in potency were observed with thiazole **15** and oxazole **16**, both of which had  $K_i$  values of  $>4$   $\mu$ M. Among the more potent compounds, an aromatic CH group is present at one of the ring positions *ortho* to the amide substituent, while in the less potent or inactive compounds, heteroatoms are present at both *ortho* positions. Examination of the crystal structure of **1** reveals that one of the *ortho*-amide positions on the pyrazole ring is directed towards the backbone carbonyl oxygen of Met-438. Thus,

**Table 2**  
SAR of pyrazole heterocyclic replacements

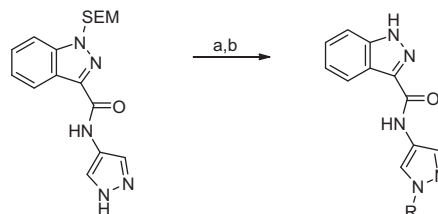
Example	R	$K_i$ (nM)
13		3.4
14		1.7
15		$>4$
16		$>4$

analogs containing an aromatic CH with a partially positively charged hydrogen atom at this position could participate in a nontraditional H-bonding interaction with this carbonyl oxygen, while compounds with an imino nitrogen or oxygen would incur lone pair repulsions, driving this sidechain into an unfavorable binding geometry. While a sulfur atom at this location might be expected to exhibit a favorable interaction with the Met438 carbonyl oxygen, the longer bond length and shorter valence angle of the sulfur would be expected to result in an altered bond vector to the cyanobenzyl group, effectively moving it away from a close edge-to-face stacking interaction with Phe437. Additionally, the negatively charged imino ring nitrogen on **15** would be expected to electrostatically clash with the neighboring amide carbonyl oxygen in the amide linker if the molecule is placed in a similar conformation as observed with **1**, driving the inhibitor into a conformation not tolerated by the protein active site.

Modifications of the cyanobenzyl moiety were then prepared using Mitsunobu couplings as described in Scheme 3 (Table 3).<sup>14</sup> Mono-substitution of the methylene carbon was well tolerated. Potency was somewhat sensitive to chirality of the benzyl substituent, as the *S* enantiomer (**19**) proved 5-fold more potent than the *R* (**18**). Disubstitution resulted in a 30-fold loss in potency (compare **17** and **19**). Changes on the cyanophenyl ring were well tolerated. Removing the cyano moiety or moving it to the *para* position proved to be potency neutral. Replacement with a chlorine or dimethylaminomethyl moiety also resulted in equipotent analogs. On one hand, this is not surprising given the projection of this ring into a solvent accessible region of the protein. However, given the apparent edge to face interaction of this ring with Phe-437 observed in the X-rays, sensitivity to electron density might have been expected.<sup>8</sup>

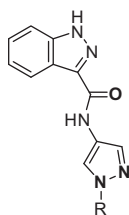
Prompted by the high potency of **19**, further exploration of methylene substitution was initiated in the context of the 6-pyrazolo-indazole subseries (Table 4). While ethyl substitution was well tolerated, polar substituents such as tertiary amines and tertiary alcohols (**27**–**30**) were preferred, with the most potent compound, *S* enantiomer **28**, demonstrating a  $K_i$  of 0.1 nM. Potency was again dependent on chirality as the *R* antipode **27** was 10-fold less potent. Inspection of the crystal structures of **27** and **28** (Fig. 4) shows that in both cases, the *N,N*-dimethylaminoethyl group projected into solvent, consistent with the preference for polar substituents at the benzylic position. For the *S* enantiomer **28**, this enforces the benzyl geometry required for edge to face  $\pi$  stacking with Phe-437. However, for the *R*-enantiomer **27** to project the dimethylaminoethyl group out to solvent, the pyrazole ring rotates 180° relative to the *S*-enantiomer, moving the benzyl moiety beyond  $\pi$  stacking distance with Phe-437 into a hydrophobic packing interaction with Ile-369. The difference in potency between the enantiomers is likely a result of the difference in free energy between these two interactions.

Cellular potencies of selected compounds was measured using a Jurkat line in which phosphorylated phospholipase C- $\gamma$ 1 (PLC  $\gamma$ -1) levels were quantitated after treatment with compound (Table 5).<sup>14</sup>



Reagents and Conditions: a) ROH, PPh<sub>3</sub>, DEAD, DCM; b) TFA, DCM

**Scheme 3.** Parallel synthesis of cyanobenzyl modifications.

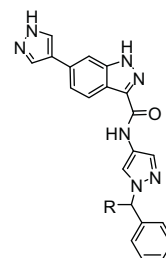
**Table 3**  
SAR of cyanobenzyl replacements

Example	R	K <sub>i</sub> (nM)
17		381
18		53
19		11
20		36
21		27
22		35
23		44

In general, cell-based and biochemical potencies were well correlated. For instance, the 20-fold increase in biochemical activity of **11** versus **1** translated to a 20-fold increase in cellular potency. Comparison of **30** and **11** showed a similar effect, as a 4-fold difference in biochemical potency tracked with a 5-fold difference in cellular potency. An exception was **28**, which is effectively equipotent to **11** in the cell assay despite being 8-fold more potent biochemically.

As the series progressed, compounds were selected for kinase selectivity assessment and in vivo pharmacokinetic studies. Selectivity testing for **1** and **28** were conducted at Invitrogen<sup>10</sup> by examining compounds at a single concentration corresponding to roughly 100× ITK K<sub>i</sub> against a panel of 75 kinases. The initial HTS hit **1** showed >50% inhibition against 18 kinases and >85% inhibition against JAK2, FLT3, MSK, PAK4, RET, and TRK. Compound **28**, which was 100-fold more potent than **1** against ITK, demonstrated >50% inhibition against 7 kinases and >85% inhibition against only FLT3. Representative compounds were also screened against LCK, a TEC kinase upstream of ITK in the T-cell receptor signaling pathway. This series consistently demonstrated >100-fold selectivity against LCK, increasing our confidence that cellular pathway inhibition was being driven by ITK interference.

Pharmacokinetic measurements of **1**, **11**, **28**, and **30** were taken in rat (Table 6). Compound **1** displayed a high in vivo clearance of

**Table 4**  
SAR of benzylic substituents

Example	R	K <sub>i</sub> (nM)
24		1.0
25		0.56
26		6.6
27		0.93
28		0.1
29		0.8
30		0.23

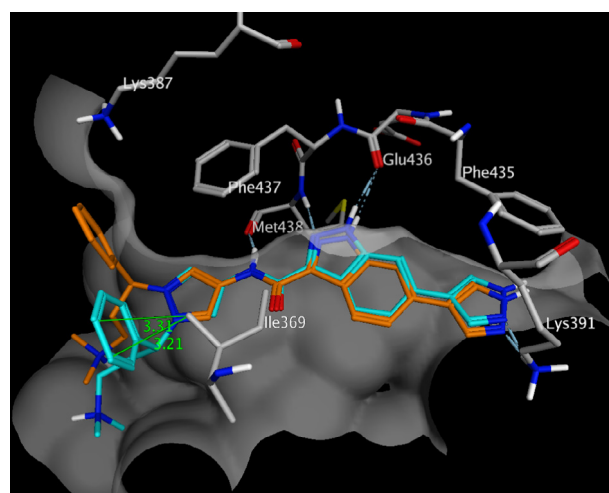


**Figure 4.** Co-crystal structures of **27** (cyan, resolution 2.8 Å, PDB code 4PPC) and **28** (orange, resolution 2.9 Å, PDB code 4PPB) with the kinase domain of ITK. For clarity, only residues from the co-crystal structure of **27** are shown. A solvent accessible surface from this complex is included. Protein–ligand hydrogen bonds are denoted by dashed lines with cylinders. Distances (Å) between the 3' methyl of Ile-369 and the closest benzyl phenyl carbons of less potent enantiomer **27** are shown in green.

**Table 5**  
Cellular potencies of selected indazoles

Example	K <sub>i</sub> (nM)	pPLCγ IC <sub>50</sub> (μM)	MDCK P <sub>app</sub> (A:B/B:A)	Log D 7.4
1	15	4.6	6.7/13.6	3.0
11	0.8	0.231	0.7/10	3.2
28	0.1	0.173	0.3/7	1.9
30	0.23	0.044	2.4/14	3.4

115 mL/min/kg and no oral bioavailability. Both **11** and **28** had much lower IV clearance relative to **1**, but demonstrated no oral bioavailability, presumably because of their low permeabilities.

**Table 6**  
Pharmacokinetic parameters of selected indazoles

Example	Route (dose)	AUC (h $\mu$ M)	$t_{1/2}$ (h)	Cl (mL/min/kg)	%F	MDCK $P_{app}$ (A:B/B:A)
1	IV (1 mg/kg)	0.42	0.26	115	—	6.7/13.6
	PO (5 mg/kg)	—	—	—	0	—
11	IV (1 mg/kg)	1.8	1.3	20	—	—
	PO (5 mg/kg)	—	—	—	0	0.7/10
28	IV (1 mg/kg)	0.837	5.7	44	—	—
	PO (5 mg/kg)	—	—	—	0	0.3/7
30	IV (1 mg/kg)	2.5	1.8	11	—	—
	PO (5 mg/kg)	—	2.6	—	9	2.4/14

In contrast, **30** demonstrated moderate MDCK permeability and this translated to low, but measureable, oral exposure.

By pursuing a structure-based design approach, an HTS-derived indazole hit was evolved into an ITK inhibitor series that demonstrated sub-nanomolar biochemical and low nanomolar cellular potencies, with good kinase selectivity. However, optimized compounds consistently demonstrated poor pharmacokinetic properties. Lead optimization efforts to improve pharmacokinetics will be discussed in future communications.

## Acknowledgments

Mengling Wong, Michael Hayes and Chris Hamman are gratefully acknowledged for the purification of all compounds described in this manuscript, and Dr. Baiwei Lin is acknowledged for the determination of logD for all compounds.

## Supplementary data

Supplementary data (full torsion profiles of 6-(1H-pyrazol-4-yl)-1H-indazole and both tautomeric forms of 6-(1H-pyrazol-3-yl)-1H-indazole. Experimentals for Schemes 1–3. Experimentals for X-ray crystallography.) associated with this article can be found, in the online version, at <http://dx.doi.org/10.1016/j.bmcl.2014.04.023>.

## References and notes

- Felices, M.; Falk, M.; Kosaka, Y.; Berg, L. J. *Adv. Immunol.* **2007**, *93*, 145.
- Sakaguchi, S.; Benham, H.; Cope, A. P.; Thomas, R. *Immunol. Cell Biol.* **2012**, *90*, 277.
- Mueller, C.; August, A. J. *Immunol.* **2003**, *170*, 5056.
- Schaeffer, E. M.; Debnath, J.; Yap, G.; McVicar, D.; Liao, X. C.; Littman, D. R.; Sher, A.; Varmus, H. E.; Lenardo, M. J.; Schwartzberg, P. L. *Science* **1999**, *284*, 638.
- For small-molecule inhibitors of ITK, see: (a) Das, J.; Liu, C.; Moquin, R. V.; Lin, J.; Furch, J. A.; Spengel, S. H.; McIntyre, K. W.; Shuster, D. J.; O'Day, K. D.; Penhallow, B.; Huang, C.-Y.; Kanner, S. B.; Lin, T.-A.; Dodd, J. H.; Barrish, J. C.; Wityak, J. *Bioorg. Med. Chem. Lett.* **2006**, *16*, 2411; (b) Lin, T. A.; McIntyre, K. W.; Das, J.; Liu, C.; O'Day, K. D.; Penhallow, C.-Y.; Whitney, G. S.; Shuster, D. J.; Xia, X.; Townsend, R.; Postelnek, J.; Spengel, S. H.; Lin, J.; Moquin, R. V.; Furch, J. A.; Kamath, A. V.; Zhang, H.; Marathe, P. H.; Perez-Villar, J. J.; Doweyko, A.; Killar, L.; Dodd, J. H.; Barrish, J. C.; Wityak, J.; Kanner, S. B. *Biochemistry* **2004**, *43*, 11056; (c) Snow, R. J.; Abeywardane, A.; Campbell, S.; Lord, J.; Kashem, M. A.; Khine, H. H.; King, J.; Kowalski, J. A.; Pullen, S. S.; Roma, T.; Roth, G. P.; Sarko, C. R.; Wilson, N. S.; Winter, M. P.; Wolak, J. P.; Cywin, C. L. *Bioorg. Med. Chem. Lett.* **2007**, *17*, 3660; (d) Moriarty, K. J.; Winters, M.; Qiao, L.; Ryan, D.; Desjarlis, R.; Robinson, D.; Cook, B. N.; Kashen, M. A.; Kaplita, P. V.; Liu, L. H.; Farrell, T. M.; Khine, H. H.; King, J.; Pullen, S. S.; Roth, G. P.; Magolda, R.; Takahashi, H. *Bioorg. Med. Chem. Lett.* **2008**, *18*, 5537; (e) Winters, K. M. P.; Robinson, D. J.; Khine, H. H.; Pullen, S. S.; Woska, J. R., Jr.; Raymond, E. L.; Sellati, R.; Cywin, C. L.; Snow, R. J.; Kashem, M. A.; Wolak, J. P.; King, J.; Kaplita, P. V.; Liu, L. H. *Bioorg. Med. Chem. Lett.* **2008**, *18*, 5541; (f) Riether, D.; Zindell, R.; Kowalski, A., et al. *Bioorg. Med. Chem. Lett.* **2009**, *19*, 1588; (g) Lo, H. Y.; Bentzien, J.; Fleck, R. W.; Pullen, S. S.; Khine, H. H.; Woska, J. R.; Kugler, S. Z.; Kashen, M. A.; Takahashi, H. *Bioorg. Med. Chem. Lett.* **2008**, *18*, 6218; (h) Charrier, J. D.; Miller, A.; Kay, D. P.; Brenchley, G.; Twin, H. C.; Collier, P. N.; Ramaya, S.; Keily, S. B.; Durrant, S. J.; Knegtel, R. M.; Tanner, A. J.; Brown, K.; Curno, A. P.; Jimenez, J. M. J. *Med. Chem.* **2011**, *54*, 2341; (i) Herdemann, M.; Weber, A.; Jonveaux, J.; Jonveaux, J.; Schwoebel, S.; Heit, I. *Bioorg. Med. Chem. Lett.* **2011**, *21*, 1852; (j) McLean, L. R.; Zhang, Y.; Zaidi, N.; Bi, X.; Wang, R.; Dharanipragada, R.; Jurcak, J. G.; Gillespy, T. A.; Zhao, Z.; Musick, K. Y.; Choi, Y. M.; Barrague, M.; Peppard, J.; Smicker, M.; Duguid, M.; Parkar, A.; Fordham, J.; Kominos, D. *Bioorg. Med. Chem. Lett.* **2012**, *22*, 3296; (k) Zapf, C. W.; Gerstenberger, B. S.; Xing, L.; Limburg, D. C.; Anderson, D. R.; Caspers, N.; Han, S.; Aulabaugh, A.; Kurumbail, R.; Shaky, S.; Li, X.; Spaulding, V.; Czerwinski, R. M.; Seth, N.; Medley, Q. G. *J. Med. Chem.* **2012**, *55*, 10047; (l) Alder, C.; Ambler, M.; Campbell, A.; Champigny, A.; Deakin, A.; Harling, J.; Harris, C.; Longstaff, T.; Lynn, S.; Maxwell, A.; Mooney, C.; Scullion, C.; Singh, O.; Smith, I.; Somers, D.; Tame, C.; Wayne, G.; Wilson, C.; Woolven, J. *ACS Med. Chem. Lett.* **2013**, *4*, 948; (m) Harling, J.; Deakin, A.; Campos, S.; Grimley, R.; Chaudry, L.; Nye, C.; Polyakova, O.; Bessant, C.; Barton, N.; Somers, D.; Barrett, J.; Graves, R.; Hanns, L.; Kerr, W.; Solari, R. J. *Biol. Chem.* **2013**, *288*, 28195; For a recent review on ITK inhibitors, see: (n) Charrier, J.-D.; Knegtel, R. M. A. *Expert Opin. Drug Discov.* **2013**, *8*, 369.
- Biochemical assay conditions*: The enzyme reaction was carried out in a final 4- $\mu$ L reaction volume in 1536-well black MAKO COP plates (Aurora Biotechnologies). Phosphorylation of the peptide substrate biotin-EQEDPEGIYGVLF-NH<sub>2</sub> (American Peptide Company, Sunnyvale CA) was initiated by the addition of 2  $\mu$ L 800 nM peptide substrate and 40  $\mu$ M ATP into 2  $\mu$ L 2 nM full-length ITK (Invitrogen) with library compounds in kinase reaction buffer (50 mM HEPES pH 7.2, 15 mM MgCl<sub>2</sub>, 0.005% Brij-35, 2 mM DTT). The reaction mixture was incubated for 1 h at ambient temperature prior to the addition of 2  $\mu$ L detection reagent containing 6 nM Europium cryptate-labeled PT66 antibody and 200 nM streptavidin XL-665 (Cisbio) in detection buffer (50 mM HEPES pH 7.2, 0.1% BSA, 0.5 M KF, 40 mM EDTA). The final reaction mixture was incubated at ambient temperature for 2 h. The signal measurement was performed using a ViewLux reader (Perkin Elmer) via excitation wavelength of 320 nm and emission wavelengths of 618 and 671 nm. The HTRF ratio was determined using the following equation:  $\text{Em671}/\text{Em618} \times 10,000$ .
- Mitsunobu, O.; Yamada, M. *Bull. Chem. Soc. Jpn.* **1967**, *40*, 2380.
- Castellano, R. K.; Diederich, F.; Meyer, E. A. *Angew. Chem., Int. Ed.* **2003**, *42*, 11.
- Lin, B.; Pease, J. H. *Comb. Chem. High Throughput Screen.* **2013**, *16*, 817.
- Selectivity screening was performed by SelectScreen® Kinase Profiling Services (Invitrogen-Life Technologies, Madison, USA).
- Miyaura, Norio; Suzuki, Akira *Chem. Rev.* **1995**, *95*, 7.
- 6-(1H-Pyrazol-4-yl)-1H-indazole was minimized in the gas phase using Jaguar (6-31 g\*\*<sup>+</sup>, DFT B3LYP basis set) using 3° increments with minimization at each step. A dihedral angle of 27° was found to be the global minimum. See Supporting information (Fig. S.1) for the full torsion profile.
- Tautomeric indazoles 6-(1H-pyrazol-3-yl)-1H-indazole and 6-(1H-pyrazol-5-yl)-1H-indazole were minimized using Jaguar (same specifications as Ref. 12). 6-(1H-Pyrazol-3-yl)-1H-indazole was found to be the more stable tautomer ( $\Delta\Delta H = 1.4$  kcal/mol), and this tautomer preferred a co-planar dihedral angle. See Supporting information (Figs. S.2 and S.3) for the full torsion profile of both tautomers.
- The ability of compounds to inhibit phosphorylation of PLC $\gamma$ 1 in Jurkat cells was determined using an immuno-detection assay that will be described in detail in a separate communication.